I S A V

Journal of Theoretical and Applied Vibration and Acoustics

journal homepage: http://tava.isav.ir

Three-dimensional underwater image formation with inverse synthetic aperture sonar

Seyyed Ali Erfani[a], Seyed Alireza Seyedin[b*]

[a]*PhD Student, Faculty of Engineering, Ferdowsi University of Mashhad, Mashhad, Iran.*

[b]*Associate Professor, Ferdowsi University of Mashhad, Mashhad, Iran*

ARTICLE INFO

Article history:
Received 14 February 2020

Received in revised form
5 June 2020

Accepted 23 October 2020

Available online 11 December 2020

Keywords:
Interferometry,

Multipath Circuits,

Emulated Bistatic,

Virtual Sources

ABSTRACT

Underwater three-dimensional imaging can be performed using several sonar sensors and interferometric methods. The problem with employng multiple sensors is the increased cost of hardware and synchronization issues. However, uncertainty reduces by using this method. An alternative way to reduce hardware is to utilize multipath circuits in the underwater environment. In this environment, multipath circuits are created by the impact of sound waves on the seafloor and sea surface. Seafloor reflections create direct-direct, direct-indirect, indirect-direct, and indirect-indirect circuits. In this paper, both methods of using and not using multipath circuits for three-dimensional imaging are presented in detail. Moreover, both approaches of using or not using virtual sources and cube target imaging will be carried out using the MATLAB software package. The type of sonar presented in this paper is an inverse synthetic aperture sonar. The results are comparable with those of the commercial systems. However, not all practical conditions are considered in this study in contrast with the commercial systems. Our contribution is the study of a novel method in three-dimensional imaging using virtual sources. This method has not been applied for this purpose before.

1. Introduction

Sonar used for underwater navigation and ranging by acoustic waves is available in various types, including inverse synthetic aperture sonar (ISAS). Inverse synthetic aperture sonar

* Corresponding author:
E-mail address: seyedin@um.ac.ir (S.A. Seyedin)

http://dx.doi.org/10.22064/tava.2021.122073.1159

is very similar to inverse synthetic aperture radar[†]. Therefore, we can come up with new ideas for solving ISAS problems by studying how ISAR works. For this reason, preliminary issues concerning inverse synthetic aperture radar will be presented and then sonar issues will be investigated.

1.1. Preliminary Topics of Inverse Synthetic Aperture Radar

Radar imaging requires high resolution and this high resolution in range is achieved with wide bandwidth and in cross range with wide antenna aperture. Wide antenna aperture can be artificially created by SAR or ISAR techniques [1]. Three-dimensional target images contain more information. Thus, having such images is of great interest and interferometry is a common way to obtain three-dimensional images of targets.

A multistatic radar (sonar) can be used for interferometry. The geometry of a three-dimensional imaging system is shown in Figure 1. It is seen that it uses one transmit antenna and two receive antennas. Coherent multistatic radar imaging is based on extending current ISAS/ISAR algorithms to a multistatic environment.

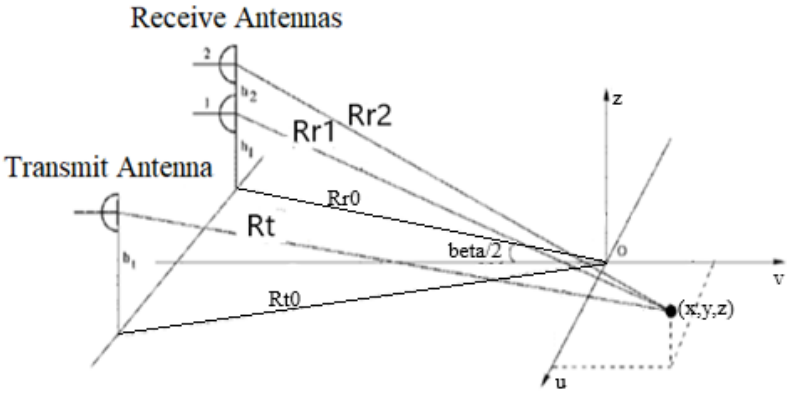

Fig. 1: Geometry of a three-dimensional imaging system.

One of the important issues that have been considered in the processing of received radar signals is that the incident wave to the ground has ground and other surface echoes called multipath. However, most radar papers on this issue have concentrated on eliminating multipath effects. In 2003, Palmer discussed the use of reflection effects of sea clutter[2]. In this paper and others that pursued it, radars that use this arrangement are called emulated bistatic radars, or EBRs for short.

1.2. Preliminary Topics of Inverse Synthetic Aperture Sonar

Increasing interest in defense applications, the offshore oil industry, and other commercial operations in the underwater environment draws more interest to underwater research. Therefore, the number of research studies and applications that are conducted to explore the underwater environments is increasing as interest in underwater research increases [3].

The use of electromagnetic waves for underwater imaging is difficult due to the absorption and scattering properties of seawater. Although recent advances in hardware, software, and algorithmic methods have led to significant improvements in the operating range of the system

[†] ISAR

[4], problems persist. For example, the attenuation coefficient associated with water absorption increases rapidly with increasing frequency [5].

Today, the importance of underwater surveying has increased, especially in offshore applications; This is due to the fact that underwater resources have been mined to a small extent. Audio imaging systems are used extensively underwater because they can be used for large-scale and small-scale exploration [6]. Imaging using sound waves is called sonar, and sonar is the acronym for sound navigation and ranging.

Acoustic imaging uses a variety of technologies such as multi-beam technology, synthetic aperture, inverse synthetic aperture, acoustic lens, and audio holography[7].

Synthetic aperture sonar (SAS) has the ability to capture images with centimetreresolution up to hundreds of meters in range [8].

In this paper, three-dimensional imaging analysis with Inverse Synthetic Aperture Sonar systems (ISAS) is discussed. Some differences between SAR (or ISAR) with SAS (or ISAS) include signal propagation speed in the environment (which is approximately 1500 m/s in SAS and it equals to the speed of light in SAR), the frequency range (which is from 5 to 650 kHz in SAS, and it is from 0.45 to 10 GHz in SAR), target speeds (which cover less than 37 km/h in SAS and space targets at SARs), and target-to-sonar distance (which ranges from 10 m to 10 km in SAS and covers about satellite distances in SARs) [9].

There has been less work done on ISAS than ISAR, and most of the work done has not been published. In the first work of 1991 [10], a two-dimensional inverse synthetic aperture imaging technique was used in which acoustic signals were reflected from simple structures in water and imaging was performed.

The three-dimensional inverse synthetic aperture sonar imaging has been done in [11]. However, they used real sources to perform three-dimensional imaging. In [9], the use of virtual sources such as seabed and sea surface, as the transmitters for inverse synthetic aperture sonar imaging, is investigated, but it does not perform three-dimensional imaging. In [12], the three-dimensional image is obtained with more details by using three-receiver sensors in the radar mode, which can be extended to the sonar mode. In a near topic, [13] uses a three-dimensional rotation of an underwater vehicle to improve two-dimensional ISAS images.

We can compare the results with existing commercial systems. For instance, by comparing our system with a commercial synthetic aperture sonar system developed by KONGSBERG, Norway, acceptable results get obtained. The name of this system is HISAS 1030. HISAS is the acronym for High Resolution Interferometric Synthetic Aperture Sonar.

This commercial system is mounted on an AUV. AUV is the HUGIN 1000 model made by the same company[14].

The operating conditions and resolutions resulting from the use of this system are described here. This system works in the frequency range of 60-120 kHz, has an up to 50 kHz system bandwidth and maximum range (each side of the vehicle) of 200 m at 2 m/s and 260 m at 1.5 m/s AUV speed. This system achieves bathymetry resolution (cell size) of 5×5 cm to 50×50 cm [14].

It is observed that the operating frequency in the simulation conditions of this article is within the frequency range of the HISAS system and its bathymetry resolution is comparable to our

simulation results; however, this commercial system is unresponsive at high ranges; also, the HISAS system is a synthetic aperture sonar, not an inverse synthetic aperture sonar, as in our article (It is necessary to mention that the synthetic aperture sonar systems are not as complex as inverse synthetic aperture sonar systems. Most of the complexity of inverse SAS systems is due to the non-cooperativity of the target motion.)

As we will see in the fourth section of this paper, our ISAS system reaches the third dimension resolution of 7 centimetres using real sources comparable to the bathymetry resolution of HISAS 1030, which is between 5×5 cm to 50×50 cm as mentioned.

We have assumed that the target is moving and it has a simple movement with no maneuvering. The use of targets with complicated movements involves time-frequency analysis, which is out of the scope of this paper.

The seabed material was assumed to be known implying that the coefficient P_0 (which will be described later in this paper) is known.

The third assumption is that we want to form the image using the monostatic configuration. So, only one transmitter/receiver is available. This structure reduces the cost of using additional transmitters.

The fourth assumption is that the target is formed from several point scatterers. The target was assumed to be simple, i.e. it is not composed of many (more than 10) scatterers. If there are many scatterers, the assignment of artifacts to the corresponding scatterers would be too time-consuming. We should compute a large number of permutations to compute the minimum variance of the scatterer-artifact distances sets. The concept of artifact will be discussed later in the paper.

Because of the military usage of ISAS, we did not have sufficient database and experimental data. Simulation conditions are not ideal and we have practical fading due to the presence of obstacles and noise. The other limitation is related to underwater limitations, such as the low speed of underwater sound wave propagation and lower available underwater bandwidth.

The paper follows with a description of underwater ray tracing in the next section. This is done both theoretically and by using simulation. The third section of the paper describes problem conditions. It includes target motion and water channel conditions. Water channel conditions are propagation loss, absorption loss, underwater sound speed, sea surface conditions, and seabed conditions. In the fourth section, the use of real sources for three-dimensional imaging is presented. In this section, the basic issues of interferometry are presented first and then the dual interferometry mode is described. Three-dimensional simulation of a cube was performed using dual interferometry in sonar mode using the MATLAB software. The fifth section describes the use of virtual sources for three-dimensional visualization. In this section, the three-dimensional simulation of the cubic target in the presence of multipath circuits is also performed. Finally, conclusions are drawn.

The objective of this paper is to do the three-dimensional imaging for inverse synthetic aperture sonar with both real and virtual sources; Our contribution is that we have used a new method for three-dimensional imaging with virtual sources.

2. Underwater ray tracing

In this section, underwater ray tracing is described theoretically and practically by using the COMSOL software package.

2.1. Underwater ray tracing theory

The wave equation describing sound propagation is derived from the equations of hydrodynamics and its coefficients and boundary conditions are descriptive of the ocean environment. The wave equation for the pressure p in cylindrical coordinates with range coordinates denoted by r = (x, y) and depth coordinate denoted by z (taken positive downward) for a source-free region is [15].

$$\nabla^2 p(\boldsymbol{r}.z.t) - \frac{1}{c^2(\boldsymbol{r}.z)}\frac{\partial^2 p(\boldsymbol{r}.z.t)}{\partial t^2} = 0 \tag{1}$$

where c(r,z) is the sound speed in the wave propagation medium. It is convenient to solve the above equation in the frequency domain by assuming a solution with a frequency dependence in the form of exp(-iωt) to obtain the Helmholtz equation,

$$\nabla^2 p(\boldsymbol{r}.z) + K^2 p(\boldsymbol{r}.z) = 0 \tag{2}$$

with

$$K^2(\boldsymbol{r}.z) = \frac{\omega^2}{c^2(\boldsymbol{r}.z)} \tag{3}$$

The Helmholtz equation for an acoustic field from a point source is [15]

$$\nabla^2 G(\boldsymbol{r}.z) + K^2(\boldsymbol{r}.z)G(\boldsymbol{r}.z) = -\delta^2(\boldsymbol{r} - \boldsymbol{r}_s)\delta(z - z_s) \tag{4}$$

where the subscript 's' denotes source coordinates. The acoustic field from a point source, G(**r**), is either obtained by solving the boundary-value problem of (4) (spectral method or normal modes) or by approximating (4) using an initial-value problem (ray theory, parabolic equation) [15].

Ray theory is a geometrical, high-frequency approximate solution to (4) of the following form:

$$G(\boldsymbol{R}) = A(\boldsymbol{R})\exp(iS(\boldsymbol{R})) \tag{5}$$

where the exponential term $S(\boldsymbol{R})$ allows for rapid variations as a function of range ($\boldsymbol{R}$) and $A(\boldsymbol{R})$ is a more slowly varying envelope that incorporates both geometrical spreading and loss mechanisms [15].

The ray theory method is computationally rapid and extends to range-dependent problems. Furthermore, the ray traces give a physical picture of acoustic paths. It is helpful in describing how sound redistributes itself when propagating long distances over paths that include shallow

and deep environments and/or mid latitudes to polar regions. The disadvantage of conventional ray theory is that it does not include diffraction [15].

There are essentially four types of models (computer solutions to the wave equation) to describe sound propagation in the sea: ray theory, the spectral method or fast field program (FFP), normal mode (NM), and parabolic equation (PE) [15]. All of these models allow for the fact that the ocean environment varies with depth. A model that also takes horizontal variations in the environment (i.e., sloping bottom or spatially variable oceanography) into account is called range-dependent [15]. For high frequencies (a few kilohertz or above), ray theory is the most practical model. The other three model types are more applicable at lower frequencies (below 1 kHz). The wave solution is the most accurate and should probably be used in all cases where the calculation is still feasible and/or practical [15].

One of the fundamental rules that govern paths of underwater rays is Snell's law [15

$$\frac{\cos(\theta(z))}{c(z)} = constant \tag{6}$$

This equation relates ray angle $\theta(z)$ with respect to the horizontal surface to the local sound speed c(z) at depth z. This equation requires a smaller angle with the horizontal surface for higher sound speeds. This implies that sound bends away from regions of high sound speed. In other words, sound bends toward regions of low sound speed [15].

In general, the ocean can be thought of as an acoustic waveguide. This waveguide physics is particularly evident in shallow water (inshore out to the continental slope, typically to depths of a few hundred meters) [15].

In the next sub-section, underwater ray tracing is performed using the COMSOL 5.4 software package.

2.2. Underwater ray tracing using simulation

Underwater ray tracing was performed before in the BELLHOP program [16]. BELLHOP is a beam tracing model for predicting acoustic pressure fields in ocean environments. The beam tracing structure leads to a particularly simple algorithm. Several types of beams are implemented, including Gaussian and hat-shaped beams, with both geometric and physics-based spreading laws. BELLHOP can produce a variety of useful outputs, including transmission loss, Eigen rays, arrivals, and received time series. It allows for range-dependence in the top and bottom boundaries (altimetry and bathymetry), as well as in the sound speed profile. Additional input files allow the specification of directional sources as well as geo-acoustic properties for the bounding media. Top and bottom reflection coefficients may also be provided. BELLHOP is implemented in Fortran, Matlab, and Python and is used on multiple platforms (Mac, Windows, and Linux)[16].

In this section, we investigate the detection of underwater acoustic radiation using COMSOL 5.4 software package. The simulation parameters with COMSOL software are given in Table 1.

Table 1. Simulation parameters with COMSOL software

Parameter	Parameter Value
Source Frequency	100 (kHz)
Source Depth	50 (m)
Water Depth	100 (m)
Water Salinity	35 (gr/Lit)
Water Density	1000 (kg/m^3)
Water Temperature	8 (degC)
PH of Water	8
Water Domain Width	2000 (m)
RMS Wave Height	1 (m)
Bottom Material Speed of Sound	1575 (m/s)
Bottom Material Density	1700 (kg/m3)
Bottom Material Attenuation (1/m)	0.0066 (1/m)
End Time for Simulation	5 (s)

In this scenario, we have a monostatic sensor at 50 meters depth. The monostatic sensor acts both as a transmitter and receiver. The paths of acoustic rays are plotted versus sound speed at different depths of water. The rate of change of sound speed versus water depth is plotted in Figure 2 (a). This graph is plotted using speed at several sample depths and interpolation is used. In Figure 2 (b), the sound pressure level along the rays is plotted. Snell's law can be investigated along these paths. It can be seen that when sound speed increases by decreasing thedepth, sound rays reflected from the seabed bend away from low depth regions and bend toward deep water (The critical points of these rays are at about 1200 meters away from the sensor). However, the Ray Acoustics modelling used cannot explain all the acoustic phenomena.

It can be seen from Figure 2 (b) that at a frequency of 100 kHz (and it can be shown that generally within the range of the working frequencies of the synthetic aperture sonar), there is no reflected power at sea level.

However, at low frequencies (for example, 100 Hz), the sea surface reflects the sound beam (In addition, investigating the Rayleigh parameter [17], which will be described in the next section, confirms this result).

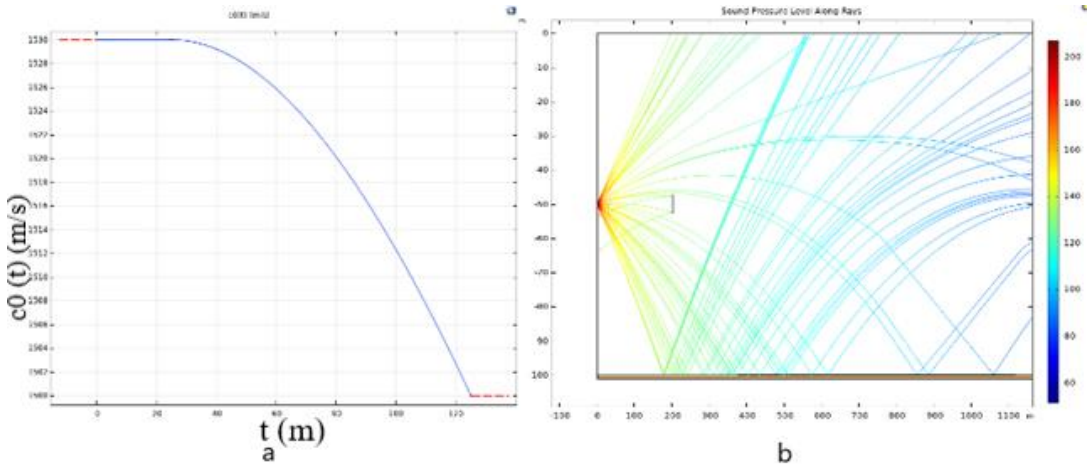

Fig. 2: Sound speed changes considered in terms of water depth (a) and Sound Pressure Level along rays (b) This Figure is obtained using parameters of Table 1.

If (as you can observe in Figure 3, which is the zoomed preview of Figure 2.b) we place a square object (or a cube object in the three-dimensional mode) with a side length of 5 meters in the distance of 200 meters from the source (we consider the object material to be stainless steel), sound radiation emitted from the source and reflected from the seabed are reflected towards the sensor after hitting the object (However, the ray acoustic model does not describe this phenomenon precisely); so, the sound wave can be sensed by the sensor and the distance to the object can be calculated.

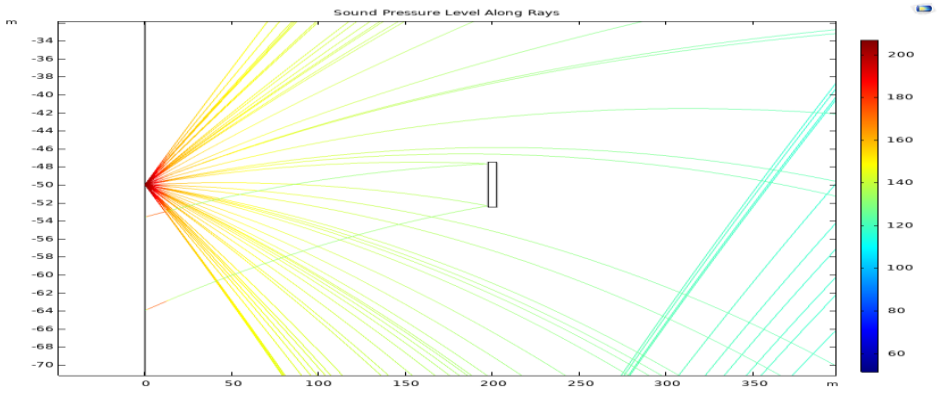

Fig. 3: The path of the acoustic ray if it hits the target. This Figure is obtained using the parameters of Table 1.

3. Problem conditions

The produced image from the underwater moving target is proportional to the target characteristics, such as how the target moves, which is described in the first subsection of this section. Water channel conditions such as spreading loss, absorption loss, underwater sound velocity, and sea surface and seabed conditions are described in the second subsection.

3.1. Target motion

A moving target motion may have six degrees of freedom, including three linear motions along three axes and three angular motions around three axes. In the inverse synthetic aperture

structure, only rotational motions produce the image. In the case that the target has translational motion, the velocity and acceleration of motion can be decomposed into two components, one aligned with the line of sight (LOS) of the target and the other perpendicular to it. The component aligned with the line of sight produces the change in the Doppler frequency; but the component perpendicular to the line of sight produces the change in the viewing angle, which has the same effect as the rotational motion of the target.

When the target has roll, pitch, and yaw motions, the combined rotational vector Ω. determines the Doppler frequency of a definite scatterer in the target. According to Figure 4, the effective rotational vector Ω_{eff}, is a vector perpendicular to i, the line of sight unit vector, and it is located on a surface on which the vectors Ω and i are located. Therefore, the reflection surface of the target (Image Projection Plane) is defined as a surface to which Ω_{eff} is perpendicular and vector i is located.

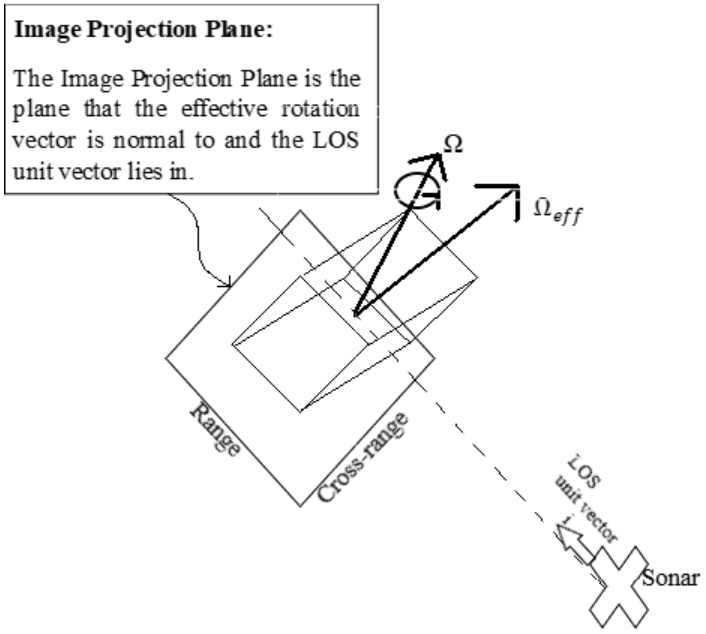

Fig. 4: Image Projection Plane (IPP) in the ISAS

In the standard motion compensation process, by doing the range correction, the scatterers will be located in the same range cells and the Doppler frequency shift remains constant by performing phase correction. Thus, after doing motion compensation, all of the target scatterers will move with the same velocity according to a constant Doppler frequency shift. Moreover, according to the constant range, they will move in a circular path. If the target has a smooth motion, the standard motion compensation method using Fourier transform is enough for producing a concentrated image of the target.

However, if the target has complex motions involving scatterers' shift from the range and time-varying Doppler frequency shift, the standard method based on Fourier Transform is not enough for producing an appropriate image. In this case, we should use more complex methods and time-frequency transforms. However, the sea targets considered usually do not have complex motions.

3.2. Water channel conditions

Underwater moving target imaging by inverse synthetic aperture sonar is related to water channel conditions. The most important effective water channel parameters that affect image formation are described in the following sub-sections.

3.2.1 Spreading loss

In the acoustic wave propagation field, one of the most effective phenomena is the loss caused by the geometric propagation of underwater waves. This loss is spherical in deep water and cylindrical in shallow water. Actually, the loss is categorized into spherical and cylindrical according to the distance from the source point [3].

If vertical propagation reaches its limits imposed by the seafloor and sea surface, then from that point on, cylindrical propagation starts for horizontal propagation. For cylindrical loss, signal attenuation is proportional to the reciprocal of squared distance and for cylindrical loss, signal attenuation is proportional to reciprocal of distance [3].

3.2.2. Absorption loss

During underwater wave propagation, some sound energy is absorbed by water. The absorption rate is proportional to wave frequency and propagation environment characteristics like pure water adhesion, amount of magnesium sulfate and boric acid in water [5].

Overall, the absorption loss effect is negligible at source frequencies lower than 1 kHz; This effect is negligible to tens of kilometers at about 10 kHz; It is negligible to about one kilometer at about 100 kHz and is negligible to less than 100 meters at megahertz where it has a low effect [5].

3.2.3. Underwater sound velocity

Underwater acoustic properties, such as paths along which sound from localized source trips, are mainly dependent on underwater sound speed structure.

Underwater sound speed can be found by using various formulas. In[18], long-range acoustic transmissions made in conjunction with extensive position determinations have been used to test the accuracy of equations used to calculate sound speed from pressure which is a function of depth z in water, temperature (T), and salinity (S).

A simple formula for the speed of sound is given in Equation (7) [17].

$$c = 1449.2 + 4.6T - 0.055T^2 + 0.00029T^3 + (1.34 - 0.01T)(S - 35) + 0.016z \tag{7}$$

where in (7), z, T, and S are equal to depth, temperature, and salinity, respectively.

However, the sound speed change is ignored in our study.

3.2.4 Sea surface and seabed conditions

Sea surface and seabed can act both as a reflector and scatterer of sound waves. The amount of reflection or scattering of sea surface depends on wave altitude, sound frequency, and incidence angle of the wave with the surface. However, the amount of scattering becomes less and the amount of reflection becomes more as the sea surface becomes flatter [17].

A criterion for roughness or smoothness of a surface is given by Rayleigh parameter, defined as [17],

$$R = kHsin(\theta) \tag{8}$$

where k is the wave number $\frac{2\pi}{\lambda}$, H is the rms wave height (crest to trough), and θ is the grazing angle. When R<<1, the surface is preliminary a rejector and produces a coherent reflection at the specular angle equal to the angle of incidence. When R>>1, the surface acts as a scatterer, sending incoherent energy in all directions.

The seabed has the same effect as sea surface. However, there is more complexity in the case of the seabed as a result of diversity and multiplicity in layers. As the seabed becomes flatter and harder, the reflection becomes more under similar conditions.

4. Using real sources for three-dimensional imaging

This section presents the use of more sensors for three-dimensional imaging since the basic method for three-dimensional interferometric imaging is interferometry. Basics of interferometry are presented first and then the number of sensors is increased and this simulation is performed in the sonar mode.

4.1. Basics of interferometry

The geometry of a three-dimensional imaging system is illustrated in Figure 1. The phase difference of the received signals of receivers 1 and 2 is related to the difference in the distances of Rr1 and Rr2. The third dimension of each point of the target is related to the phase difference of the signals by a second-degree equation (9) using Taylor series expansion and the method described in detail in [19] as follows:

$$(1+x)^{\frac{1}{2}} = 1 + \left(\frac{1}{2}\right)x - \left(\frac{1}{8}\right)x^2 + \cdots \tag{9}$$

4.2. Using multiple receiver sensors

More details of the target, such as the target's effective rotation vector and target's rotation value, can be obtained by using the method described in detail in [12]. If three receivers and one transmitter are used (where one sensor or the central sensor plays both roles), it is called dual interferometry. This is due to the fact that interferometry can be done with the central sensor and each of the other two receivers.

4.2.1. The geometry of Dual Interferometric System

The geometry of the dual interferometry system is shown in Figure 5, in which the AC antenna, or central antenna, is both transmitter and receiver, and the rest of the antennas, i.e., AH and AV antennas, are the only receivers. In the case of the object, two constant and variable coordinates y and x are defined. ϕ, is the rotation degree of the reference system x relative to the fixed reference system on the sensor, ξ.

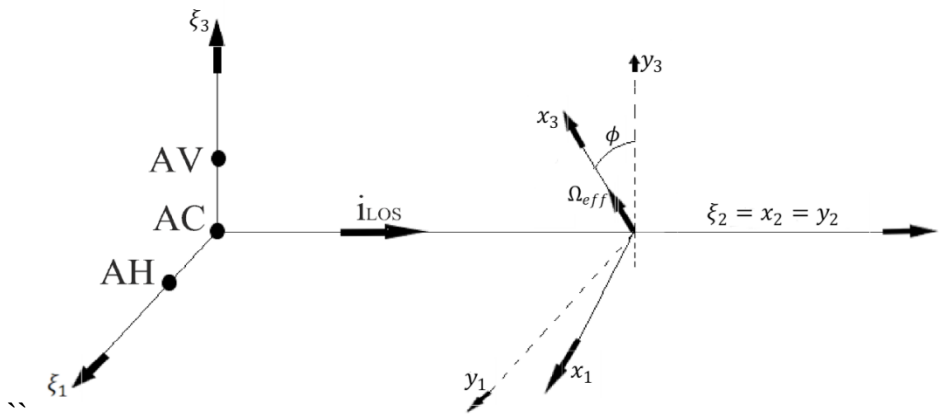

Fig. 5: Geometry of ISAR system with three receivers (Dual Interferometric Mode)

4.2.2. Cube target simulation using dual interferometry mode

In this section, an idea simulated in [12] for the radar mode is simulated for the sonar mode, considering a half-meter cube target, using MATLAB software. Simulation is done with simulation parameters shown in Table 2. The results of simulations using step frequency signal and the range Doppler image formation algorithm are presented in Figure 6, where the result of ISAS imaging which is a two-dimensional image in the range and cross-range dimensions (as the ISAR image), is presented in addition to the target model. As there are three receiving antennas (One of the antennas has both roles of transmitting and receiving), we could have two bistatic images, one for the AV and one for the AH antenna (in addition to a monostatic image corresponding to the AC antenna). In Figure 6, the bistatic image corresponding to AV antenna has been shown. As it is observed in Figure 6.b, the 8 points related to the vertices of the cube, in pairs, overlap; Therefore, only four bright spots can be seen in the figure. Then, considering the values of the third dimension derived from the implementation of the method described in [12] as mentioned in general in 4.1, the approximate three-dimensional image is plotted (Figure 7).

Table 2. Cube Target Simulation Parameters Using Dual Interferometry Mode

Parameter	Parameter Value	Parameter	Parameter Value	Parameter	Parameter Value
Sound Speed	1500 (m/s)	Carrier Frequency	100 (kHz)	Target Velocity	10 (km/h)
Number of Signal's Frequency Steps	128	Cube Side Length	0.5 (m)	Transmitted Signal's Velocity	10 (kHz)
Number of Signal's Time Sweeps	128	R_0	100 (m)	Amplitude and period of target oscillation parameters (pitch, roll, yaw)	(15,7,3) degrees and (10,12,12) seconds
Observation Time	1 (s)	d_V and d_H	15 (mm)	The amount of target rotational parameters (PHI,NI,MU)	(0,15,90) degrees

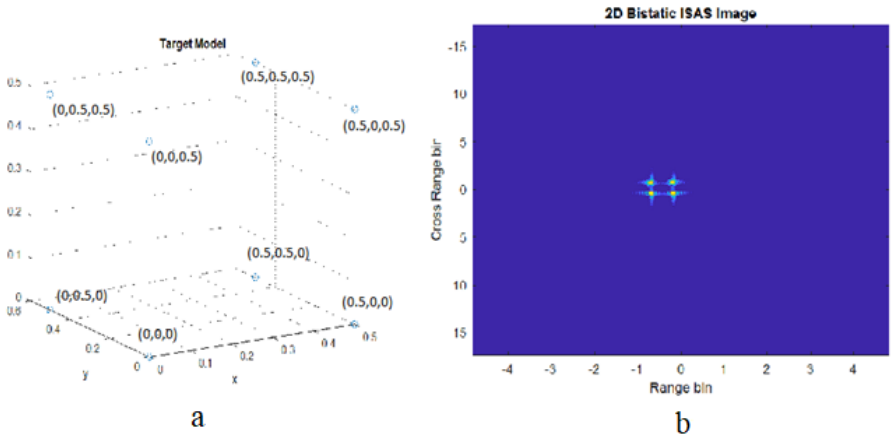

Fig. 6: a) The target model simulated using MATLAB software. b) Two-dimensional bistatic image obtained from simulation. The bistatic image is related to the AV receiver antenna.

It is found that the mean absolute value of the obtained altitude error is 6.78 cm (about 7 cm), when we consider the accurate amounts of the altitudes (This amount is obtained by averaging the scatterer height errors. We have obtained the scatterer heights by simulating the dual interferometric method with the MATLAB software). The reconstructed three-dimensional image is shown in Figure 7. In this figure, the approximate amounts of the altitudes are used. According to defining a threshold to obtain the position of the scatterers, for each point target, a clean point (without side lobe) is obtained. As it can be observed from Figure 7, by looking at all of the points at a glance, the shape of a cube can be estimated.

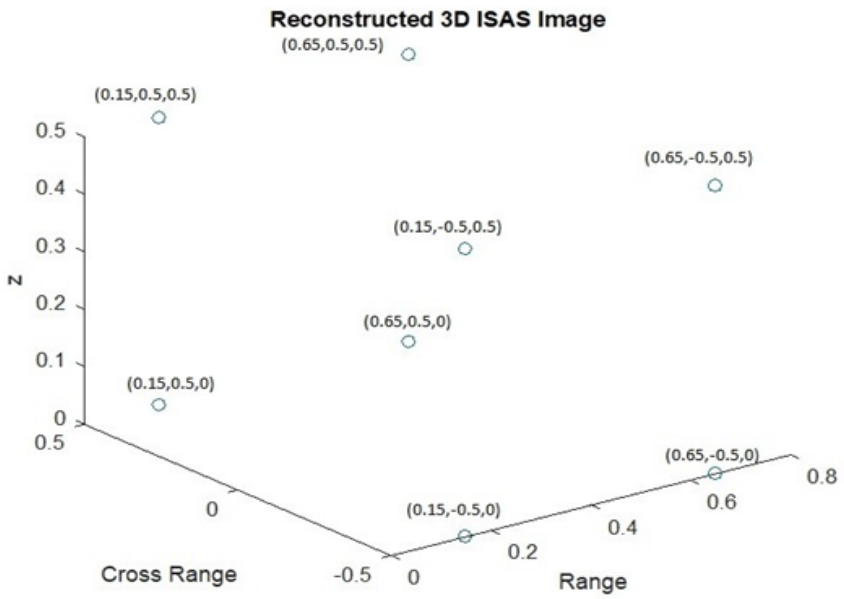

Fig. 7: Reconstructed three-dimensional ISAS image

5. Using virtual sources for three-dimensional image formation

This section presents the effective use of multipath circuits for three-dimensional image formation. Multipath circuits can be used to improve two-dimensional image quality (as in [9, 20]) or three-dimensional image formation (as in [21]). Both of these are listed in the first and second sections, respectively.

5.1. Use multipath to improve two-dimensional image quality

Formation of a bistatic image using sea clutter where sea clutter acts as a virtual transmitter is discussed in [20]. Therefore, we will have three images instead of one ISAR image. The reason we have three images is that sea clutter generates two virtual (quasi-transmitter) antennas (The transmitted signal can hit the target directly and returns directly toward the sensor, or hit the target directly and then hit the sea and return, i.e., indirectly. This implies that the entire route is direct-indirect, or vice versa, the indirect-direct path, or both signal paths are indirect (i.e., the whole path is indirect-indirect.). Two weaker images (artifacts) are created due to the indirect path next to the original image, the weakest being the indirect-indirect path.

In [20], the original image is separated from two related artifacts by cropping. Then, by taking a 2D inverse Fourier transform of each of the three cropped images and adding a translational motion phrase (previously deleted in motion compensation), three ISAR signals will be generated. This variety of signals results in improved image quality [20]. Multipath circuits were used in [9] in a different way to improve the 2D image quality of inverse synthetic aperture sonar.

5.2. Use multipath circuits to form a three-dimensional image

Figure 8 shows the emulated multistatic arrangement and equivalent virtual antennas. The virtual antennas are EMR (Emulated Monostatic Radar) and EBR (Emulated Bistatic Radar), with the EMR on the E point and EBR approximately on the B-point. The real antenna is MR (Monostatic Radar). Each of the three pairs of MR-EBR, EBR-EMR or MR-EMR images could be used for interferometry [21].

For example, MR and EMR antennas are selected. The received signal corresponding to these antennas has a phase difference which has a linear relation to the height of the scatterers. This linear relation is obtained after simplifying the theoretical expressions for the phase difference of these two signals by the method described in [21].

In this subsection, the formulas for three-dimensional images are first described in part 1. In part 2, we investigate the simulation of a cubic target. For a detailed investigation, obtaining the third dimension of the point scatterers is described in part 3.

5.2.1 Formulas for obtaining the third dimension of each scatterer from the distance of each scattering point to the corresponding artifact

When the target moves at a low elevation angle over a reflecting surface, effects like reflection, refraction, and diffraction can be taken into account by considering a complex quantity F called "pattern propagation factor" defined as the ratio between the electromagnetic (EM) field incident on the target in multipath condition and in free-space propagation. By referring to the simple geometry of Figure 8 and assuming that the diffuse scattering component is negligible, the quantity F is usually expressed by [22]:

$$F(f.\mathbf{R}) = [1 + g(\theta_2)\Gamma DS exp(j\gamma)] \tag{10}$$

where g(θ) is the antenna pattern function, **R** is the vector that locates the target position and $\gamma = \frac{-2\pi f}{c}\Delta R[\mathbf{R}]$ is the phase delay due to the length difference $\Delta R[\boldsymbol{R}]$ between the direct and reflected ray paths. The other coefficients are as follows [22]:

1. The **Fresnel coefficient** Γ quantifies the reflection from a smooth plane surface. It depends on the grazing angle ψ.
2. 2) The **divergence factor** D includes the divergence phenomenon due to earth curvature. (which is negligible in the sonar case because of the short distances).
3. 3) The coefficient S is the rms value of the **specular scattering coefficient** ρ_s that takes the roughness of the reflecting surface into account.

By considering the two-way transmission of radar, the spectrum of the received signal in the presence of multipath circuits is obtained by multiplying the multipath-free received signal by the factor $F^2(f.\boldsymbol{R})$ [22].

The product $g(\theta)\Gamma DS$ is shown by P_0 in this paper and it is assumed to be constant. In the simulations, this constant is assumed to be equal to 0.3.

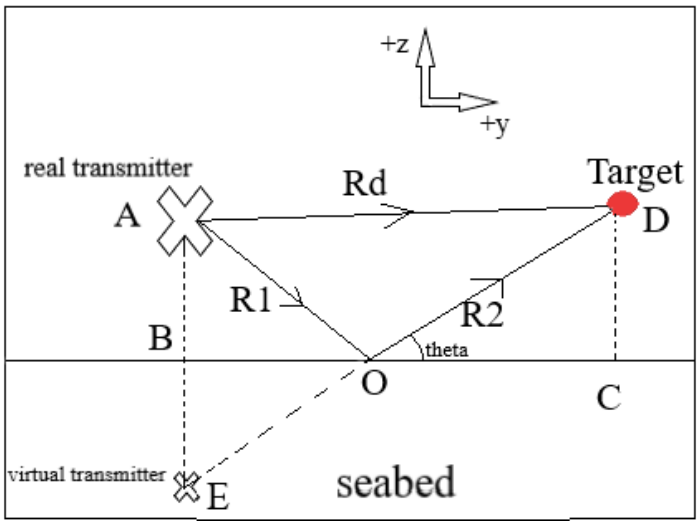

Fig. 8: Multipath geometry

The goal is to obtain the value of the first (original) artifact (in both range and cross-range directions) relative to the main scatterer (Observe Figure 9), that is, to obtain the value of the difference of the length of the return (indirect) and direct paths (This difference is found according to the approximate Equation (11), using Equations (12) and (13), by obtaining z_{01} and z_{02}.).

$$\Delta R = \alpha_0 + \beta_0 t \tag{11}$$

$$z_{01} = \frac{\beta_0 T_{obs} r_{z_1}}{\lambda_0} \tag{12}$$

$$z_{02} = \frac{\alpha_0}{2} \tag{13}$$

In Equation (11), α_0 and β_0 are the first and second parameters of the Taylor expansion of ΔR. In Equation (12), λ_0, is is the wavelength corresponding to the central frequency; r_{z1} is resolution in the cross-range dimension and T_{obs} is observation time of the sensor. See [22] for proof of these equations. Then, trigonometric relationships are used to obtain the third dimension.

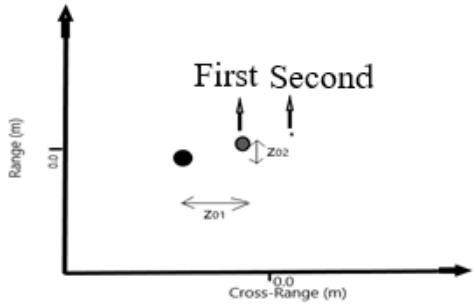

Fig. 9: The image obtained by simulating the single-scatterer mode in the presence of multipath circuits. The first artifact is clearly visible next to the scatterer (The biggest circle at the left of the image). The first and second artifacts are shown by "First" and "Second" in the figure.

5.2.2 Simulation of a cubic target

The ideas presented in [22] can be used to create a sonar image. The use of multipath circuits in sonar poses some challenges. For example, radar frequencies cannot be used in this case; Therefore, image resolution decreases with decreasing bandwidth. Moreover, the processing is not in real time due to the low speed of sound waves in water. Using COMSOL software, we demonstrated that sea-level acoustic-ray radiation echoes at the sonar frequency range are not strong enough to be used. However, reflections from the seabed can be used. Simulation conditions for simulating the cubic target are given in Table 3. For the simulation, a step frequency signal and the range Doppler image formation algorithms are used. In order to obtain the third dimension, the relationships given in [22] are used here. However, in [22], only the effects of multipath circuits were discussed rather than its use. A brief description of these formulas was given in the previous section. The two-dimensional ISAS image, using the parameters given in Table 3, is shown in Figure 10.

Table 3. Cubic target simulation parameters by ISAS in the presence of multipath circuits.

Parameter	Parameter Value	Parameter	Parameter Value
Sound speed	1500 (m/s)	Carrier Frequency	25 (kHz)
Cube Side Length	5 (m)	Target Altitude from the Seabed	25 (m)
Distance Between the Sensor and the Target (in the x dimension)	0	Transmitted Signal Bandwidth	2.5 (kHz)
Distance Between the Sensor and the Target (in the y dimension)	100 (m)	Number of Frequency Steps of the Signal	1001
Observation Time	0.5 (s)	Number of Time Sweeps of the Signal	1001
(PHI,NI,MU)	(0,0,90) degree	Sonar Sensor Altitude from the Seabed	50 (m)
Oscillation Parameters	0	Target Velocity	30 (km/h)
P_0	0.3		

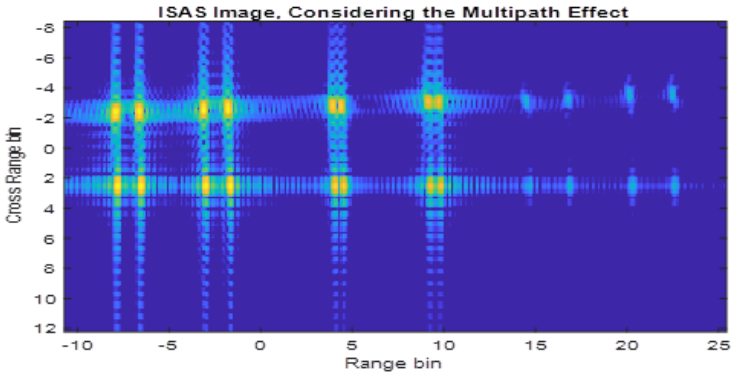

Fig. 10: Two-dimensional ISAS image consisting of a cube in the presence of multipath circuits.

There are 24 bright spots in Figure 10. The eight brighter spots (on the left of the image) belong to eight vertices. The other sixteen points belong to the first and second artifacts. The third dimension of each scatterer is obtained by using the distance of each bright point to the first artifact corresponding to it and by applying formulas given in [22].

The obtained values are 26.4, 28.02, 26.36, 28.22, 25.36, 26.25, 29.19 and 28.25. Compared with the theoretical values of the third dimension, which are 25 and 30 meters (given the 25-meter target height and the 5-meter cube length), the height error is approximately one to two meters. For the accurate estimate of this error, we have attributed each luminous point to the corresponding vertex in the cube. The reconstructed three-dimensional image is shown in Figure 11.

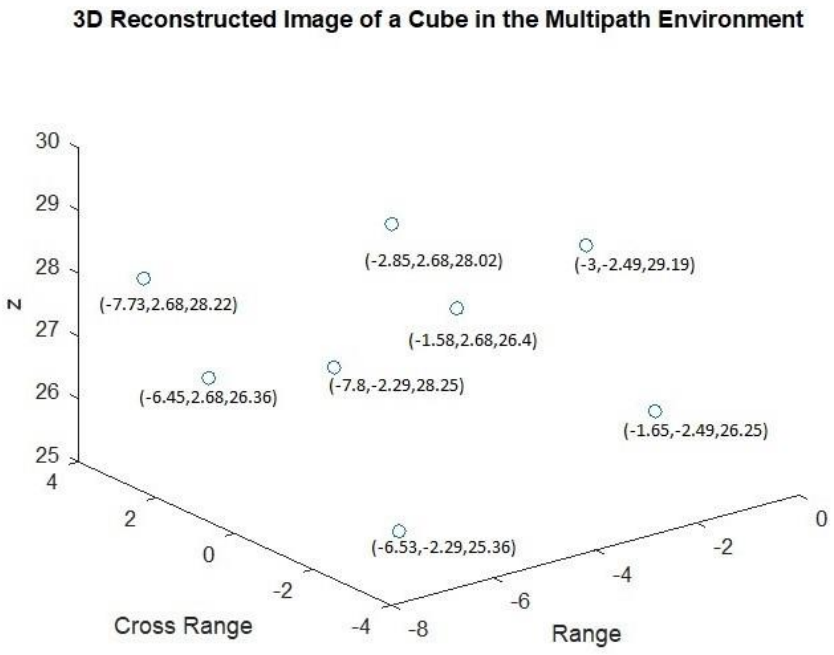

Fig. 11: The reconstructed three-dimensional image of the cube in the presence of multipath circuits

5.2.3. Precise observation of single scatterer targets

The elevation error percent when the distance between the platform and the scatterer is 500 meters is shown in Table 4 (The other simulation parameters are like Table 3).

The error percent is obtained by Equation (14).

$$error - percent = \frac{|h_{simulated} - h_{real}| \times 100}{h_{real}}) \quad (14)$$

In Equation (14), error-percent is the percentage of altitude error; $h_{simulated}$, indicates the altitude of the scatterer, obtained by the simulation and h_{real}, is the actual altitude of the scatterer. Also, $h_{simulated}$, is obtained by solving Equation (15).

$$proj\left\{\sqrt{(1+\left(\frac{h_{sonar}+h_{simulated}}{proj}\right)^2)}-\sqrt{(1+\left(\frac{h_{sonar}-h_{simulated}}{proj}\right)^2)}\right\}=\alpha_0 \quad (15)$$

In Equation (15), proj is the vector obtained by projecting the scatterer on the two-dimensional xy plane (segment BC in Figure 8). h_{sonar}, is the height of the sonar measured from the seabed and α_0 is the first component of the Taylor expansion of the difference between direct and indirect paths. Note that Equation (15), is written for the middle of the observation time (i.e. the time zero).

Table 4. Elevation error percentage when the distance between the platform and the scatterer is 500 meters.

Real scatterer altitude relative to the seabed	Altitude error percentage from simulation
10	%0.11
20	%0.05
30	%0.05
40	%0.29
50	%0.02

The altitude error values are found to be low and appropriate (the corresponding average simulation error of these five scattering heights is %0.104 relative to the seabed). Now, we reduce the distance of the sonar with the single scatterer target and set it to be 100 meters. We get the results again. In this case, the average error is %5.08. This amount is obtained by averaging the altitude errors when the altitudes are the amounts of Table 4. The graph-relating percentage of altitude errors at different distances and heights is shown in Figure 12. Different distances of the sonar sensor from the target scatterer (in the first and second dimensions of the image), in meters, are shown in circles in the first row of this Figure. Then, the average error percentage of each interval is given in rectangles in the second row. This average is obtained by averaging over 12 altitude errors at altitudes of 5 to 60 m (with 5 m steps). The variance of percentage error associated with each interval is shown in the third row. The percentage error of 500 m distances at 10 to 50 m altitudes (where the height in the fourth row is shown in circles) is given in the fifth row inside the rectangles.

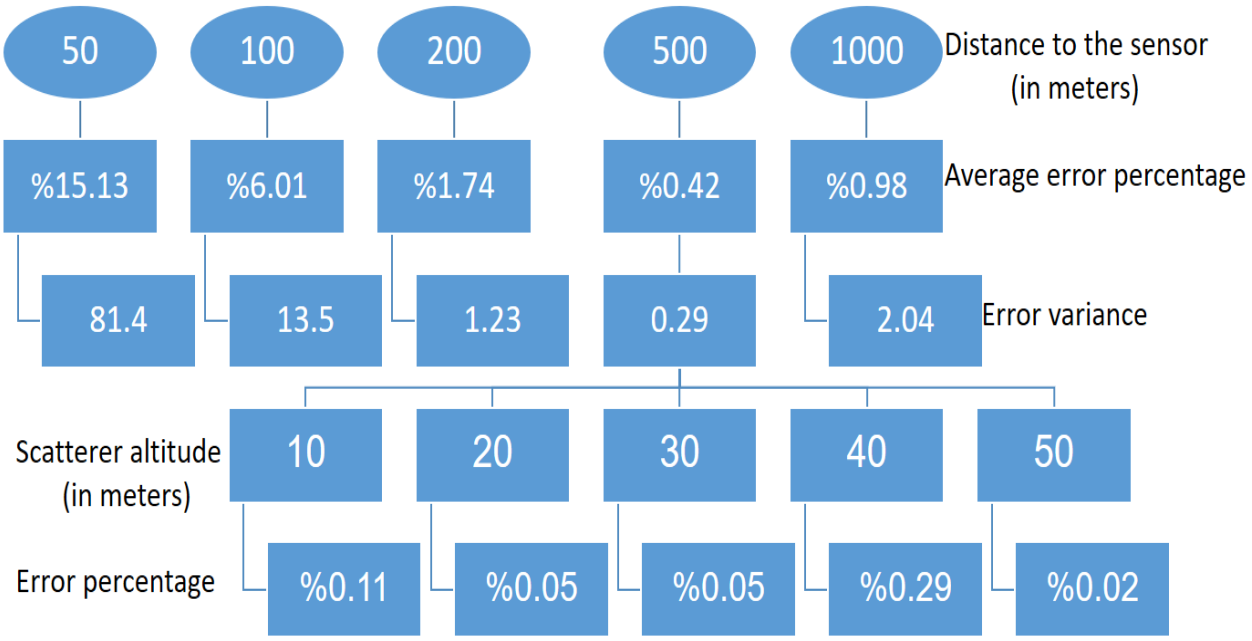

Fig. 12: Graph showing the error rate at different altitudes and distances

6. Conclusion

In this paper, three-dimensional underwater imaging by an inverse synthetic aperture sonar has been presented. Because of the similarity of the idea, papers from the inverse synthetic radar were consulted and used. The problem was investigated using real and virtual sources and in both cases and simulations were performed utilizing MATLAB software.

A new method was employed to obtain the altitude of the target scatterers in the presence of virtual sources. This method has never been applied in the literature for this purpose.

It was found that the resolution results that had been obtained using virtual sources, while the sonar distance from the target is far (about 500 m), were significantly satisfactory. However, the results were closely satisfactory if real sources were used. The results are comparable with the commercial products.

The contribution of this study is the use of virtual sources to perform interferometry in the monostatic ISAS configuration. The interferometry has been done after obtaining the distance between each scatterer and its corresponding artifact in the two-dimensional ISAS image. This method has not been used before for this purpose. However, it has been practiced for multipath cancellation.

Simulation under specific underwater conditions of the Persian Gulf is considered for future work. In addition, simulation using other image formation algorithms like back-projection method is considered. We will try to reduce the error of obtaining the third dimension of the near

field targets using the back-projection method in our future research work. Future work will also consider practical conditions like obstacles on the path and limit simulation conditions to those of the Persian Gulf. Considering more practical conditions is aimed for a future paper.

References

[1] V.C. Chen, Inverse Synthetic Aperture Radar Imaging; Principles, Institution of Engineering and Technology, 2014.
[2] J. Palmer, J. Homer, B. Mojarrabi, Improving on the monostatic radar cross section of targets by employing sea clutter to emulate a bistatic radar, in: IGARSS 2003. 2003 IEEE International Geoscience and Remote Sensing Symposium. Proceedings (IEEE Cat. No. 03CH37477), IEEE, 2003, pp. 324-326.
[3] E. Epçaçan, Underwater channel modeling for sonar applications, in, 2011.
[4] F.M. Caimi, D.M. Kocak, F. Dalgleish, J. Watson, Underwater imaging and optics: Recent advances, in: OCEANS 2008, IEEE, 2008, pp. 1-9.
[5] X. Lurton, P. Blondel, M. Collins-K., Ambient noise in the ocean, in: An Introduction to Underwater Acoustics: Principles and Applications. 2nd ed., Springer, 2010, pp. 123-165.
[6] V. Murino, A. Trucco, Three-dimensional image generation and processing in underwater acoustic vision, Proceedings of the IEEE, 88 (2000) 1903-1948.
[7] H. Guo, R. Li, F. Xu, L. Liu, Review of research on sonar imaging technology in China, Chinese journal of oceanology and limnology, 31 (2013) 1341-1349.
[8] R. Hansen, Introduction to Synthetic Aperture Sonar Systems, September 2011.
[9] J. Taghizadeh, S.A. Seyedin, Underwater moving target imaging using Multistatic Inverse Synthetic Aperture Sonar (MISAS) with virtual resources, (2015).
[10] W.K. Blake, T.D. Le, J.R. Peoples, Target interpretation using inverse synthetic aperture sonar techniques, The Journal of the Acoustical Society of America, 90 (1991) 2341-2341.
[11] P. Serafin, M. Okon-Fafara, M. Szugajew, C. Lesnik, A. Kawalec, 3-D inverse synthetic aperture sonar imaging, in: 2017 18th International Radar Symposium (IRS), IEEE, 2017, pp. 1-7.
[12] M. Martorella, D. Stagliano, F. Salvetti, N. Battisti, 3D interferometric ISAR imaging of noncooperative targets, IEEE Transactions on Aerospace and Electronic Systems, 50 (2014) 3102-3114.
[13] S. Sun, Y. Chen, L. Qiu, G. Zhang, C. Zhao, Inverse synthetic aperture sonar imaging of underwater vehicles utilizing 3-D rotations, IEEE Journal of Oceanic Engineering, 45 (2019) 563-576.
[14] T.G. Fossum, P.E. Hagen, B. Langli, R.E. Hansen, HISAS 1030: High resolution synthetic aperture sonar with bathymetric capabilities, Shallow survey, Portsmouth, NH, USA, (2008).
[15] W.A. Kuperman, P. Roux, Underwater acoustics, in: Springer Handbook of Acoustics, Springer, 2014, pp. 157-212.
[16] M.B. Porter, The bellhop manual and user's guide: Preliminary draft, Heat, Light, and Sound Research, Inc., La Jolla, CA, USA, Tech. Rep, 260 (2011).
[17] R.J. Urick, Principles of underwater sound-2, (1975).
[18] B.D. Dushaw, P.F. Worcester, B.D. Cornuelle, B.M. Howe, On equations for the speed of sound in seawater, The Journal of the Acoustical Society of America, 93 (1993) 255-275.
[19] X.J. Xu, R.M. Narayanan, Three-dimensional interferometric ISAR imaging for target scattering diagnosis and modeling, IEEE Transactions on Image Processing, 10 (2001) 1094-1102.
[20] J. Palmer, I.D. Longstaff, M. Martorella, B. Littleton, ISAR imaging using an emulated multistatic radar system, IEEE transactions on aerospace and electronic systems, 41 (2005) 1464-1472.
[21] X. Cao, F. Su, H. Sun, G. Xu, Three-dimensional In-ISAR imaging via the emulated bistatic radar, in: 2007 2nd IEEE Conference on Industrial Electronics and Applications, IEEE, 2007, pp. 2826-2830.

[22] F. Berizzi, M. Diani, Multipath effects on ISAR image reconstruction, IEEE Transactions on Aerospace and Electronic Systems, 34 (1998) 645-653.